PHYSICAL REVIEW D **95,** 052004 (2017)

Measurements of charm mixing and *CP* violation using $D^0 \to K^{\pm}\pi^{\mp}$ decays

R. Aaij *et al.*[*]
(LHCb Collaboration)

(Received 25 November 2016; published 23 March 2017)

Measurements of charm mixing and *CP* violation parameters from the decay-time-dependent ratio of $D^0 \to K^+\pi^-$ to $D^0 \to K^-\pi^+$ decay rates and the charge-conjugate ratio are reported. The analysis uses $\overline{B} \to D^{*+}\mu^- X$, and charge-conjugate decays, where $D^{*+} \to D^0\pi^+$, and $D^0 \to K^{\mp}\pi^{\pm}$. The pp collision data are recorded by the LHCb experiment at center-of-mass energies $\sqrt{s} = 7$ and 8 TeV, corresponding to an integrated luminosity of 3 fb^{-1}. The data are analyzed under three hypotheses: (i) mixing assuming *CP* symmetry, (ii) mixing assuming no direct *CP* violation in the Cabibbo-favored or doubly Cabibbo-suppressed decay amplitudes, and (iii) mixing allowing either direct *CP* violation and/or *CP* violation in the superpositions of flavor eigenstates defining the mass eigenstates. The data are also combined with those from a previous LHCb study of $D^0 \to K\pi$ decays from a disjoint set of D^{*+} candidates produced directly in pp collisions. In all cases, the data are consistent with the hypothesis of *CP* symmetry.

DOI: 10.1103/PhysRevD.95.052004

I. INTRODUCTION

The oscillation of D^0 mesons into $\overline{D}^0$ mesons, and vice versa, is a manifestation of the fact that the flavor and mass eigenstates of the neutral charm meson system differ. Such oscillations are also referred to as mixing. Charge-parity violation (*CPV*) in the superpositions of flavor eigenstates defining the mass eigenstates can lead to different mixing rates for D^0 into $\overline{D}^0$ and $\overline{D}^0$ into D^0. The LHCb experiment has previously reported measurements of mixing and *CP* violation parameters from studies of $D^{*+} \to D^0\pi_s^+$, $D^0 \to K^{\pm}\pi^{\mp}$ decays, where the D^{*+} meson is produced directly in pp collisions [1]. In this sample, referred to as "prompt," the flavor of the D^0 mesons at the production is determined by the charge of the slow pion π_s^+ from the strong decay of the D^{*+} meson. In this paper we extend the study using D^0 mesons produced in $\overline{B} \to D^{*+}\mu^- X$, $D^{*+} \to D^0\pi_s^+$, $D^0 \to K^{\pm}\pi^{\mp}$ and charge-conjugate decays [2], using pp collision data recorded by the LHCb experiment at center-of-mass energies $\sqrt{s} = 7$ and 8 TeV, corresponding to an integrated luminosity of 3 fb^{-1}. In this case, the flavor of the D^0 at production is tagged twice, once by the charge of the muon and once by the opposite charge of the slow pion π_s^+ produced in the D^{*+} decay, leading to very pure samples. The doubly tagged (DT) $\overline{B} \to D^{*+}\mu^- X$ candidates selected by the trigger are essentially unbiased with respect to the D^0 decay time, while those in the prompt sample are selected by the trigger with a bias towards higher decay times. As a result, the DT analysis allows for better measurements at lower decay times. In this paper, we first report the results of a mixing and *CPV* analysis using the DT sample, and then report the results of simultaneous fits to the DT and prompt samples.

II. THEORETICAL FRAMEWORK

The physical eigenstates of the neutral D system, which have well-defined masses and lifetimes, can be written as linear combinations of the flavor eigenstates, which have well-defined quark content: $|D_{1,2}\rangle = p|D^0\rangle \pm q|\overline{D}^0\rangle$. We follow the convention $(CP)|D^0\rangle = -|\overline{D}^0\rangle$ [3]. The coefficients p and q are complex numbers, and satisfy the normalization condition $|p|^2+|q|^2=1$. The dimensionless quantities which characterize mixing are $x=2(m_2-m_1)/(\Gamma_1+\Gamma_2)$ and $y=(\Gamma_2-\Gamma_1)/(\Gamma_1+\Gamma_2)$, where $m_{1,2}$ and $\Gamma_{1,2}$ are the masses and widths of the mass eigenstates. In the limit of *CP* symmetry, p and q are equal. To the extent that *CPV* results only from $p \neq q$, and not from direct *CPV* in the D decay amplitudes themselves, and in the limit $|1-|q/p|| \ll 1$, Wolfenstein's superweak constraint relates the mixing and *CPV* parameters [4,5]:

$$\tan\varphi = \left(1-\left|\frac{q}{p}\right|\right)\frac{x}{y}, \tag{1}$$

where $\varphi = \arg(q/p)$. Allowing for both direct and indirect *CPV*, existing measurements give $x = (0.37 \pm 0.16)\%$ and $y = (0.66^{+0.07}_{-0.10})\%$ [3]. These values are consistent with Standard Model (SM) expectations for long-distance contributions [6,7]. No evidence for *CPV* in mixing rates has been reported, and SM expectations are $\lesssim 10^{-3}$ [6–10].

We use $D^0 \to K^{\pm}\pi^{\mp}$ decays to study mixing and *CPV*. The decays $D^0 \to K^-\pi^+$ are called "right sign" (RS) and

[*]Full author list given at the end of the article.

their decay rate is dominated by Cabibbo-favored (CF) amplitudes where no direct *CPV* is expected in the SM or most of its extensions. Decays of $D^0 \to K^+\pi^-$ are called "wrong sign" (WS). Such decays do not have such a simple description. In the limit $(x, y) \ll 1$, an approximation of the WS decay rates of the D^0 and $\overline{D}^0$ mesons is

$$|\langle K^+\pi^-|H|D^0(t)\rangle|^2 \approx \frac{e^{-\Gamma t}}{2}|\mathcal{A}_f|^2\left\{R_D^+ + \left|\frac{q}{p}\right|\sqrt{R_D^+}[y\cos(\delta-\varphi) - x\sin(\delta-\varphi)](\Gamma t) + \left|\frac{q}{p}\right|^2\frac{x^2+y^2}{4}(\Gamma t)^2\right\} \quad (2)$$

and

$$|\langle K^-\pi^+|H|\overline{D}^0(t)\rangle|^2 \approx \frac{e^{-\Gamma t}}{2}|\overline{\mathcal{A}}_{\overline{f}}|^2\left\{R_D^- + \left|\frac{p}{q}\right|\sqrt{R_D^-}[y\cos(\delta+\varphi) - x\sin(\delta+\varphi)](\Gamma t) + \left|\frac{p}{q}\right|^2\frac{x^2+y^2}{4}(\Gamma t)^2\right\}. \quad (3)$$

In Eqs. (2) and (3), A_f denotes the CF transition amplitude for $D^0 \to K^-\pi^+$ and $\overline{\mathcal{A}}_{\overline{f}}$ denotes the CF transition amplitude for $\overline{D}^0 \to K^+\pi^-$. The term Γ is the average decay width of the two mass eigenstates. Denoting the corresponding doubly Cabibbo-suppressed (DCS) amplitudes $\mathcal{A}_{\overline{f}}$ for $D^0 \to K^+\pi^-$ and $\overline{\mathcal{A}}_f$ for $\overline{D}^0 \to K^-\pi^+$, the ratios of DCS to CF amplitudes are defined to be $R_D^+ = |\mathcal{A}_{\overline{f}}/\mathcal{A}_f|^2$ and $R_D^- = |\overline{\mathcal{A}}_f/\overline{\mathcal{A}}_{\overline{f}}|^2$. The relative strong phase between the DCS and CF amplitudes $\overline{\mathcal{A}}_f$ and $\mathcal{A}_f$ is denoted by δ. We explicitly ignore direct *CPV* in the phases of the CF and DCS amplitudes. As the decay time t approaches zero, the WS rate is dominated by DCS amplitudes, where no direct *CPV* is expected. At longer decay times, CF amplitudes associated with the corresponding antiparticle produce oscillations; by themselves, they produce a pure mixing rate proportional to $(\Gamma t)^2$, and in combination with the DCS amplitudes they produce an interference rate proportional to (Γt). Allowing for all possible types of *CPV*, the time-dependent ratio of WS to RS decay rates, assuming $|x| \ll 1$ and $|y| \ll 1$, can be written as [5]

$$R(t)^{\pm} = R_D^{\pm} + \sqrt{R_D^{\pm}}y'^{\pm}\left(\frac{t}{\tau}\right) + \frac{(x'^{\pm})^2 + (y'^{\pm})^2}{4}\left(\frac{t}{\tau}\right)^2, \quad (4)$$

where the sign of the exponent in each term denotes whether the decay is tagged at production as D^0 $(+)$ or as $\overline{D}^0$ $(-)$. The terms x' and y' are x and y rotated by the strong phase difference δ, and $\tau = 1/\Gamma$.

The measured ratios of WS to RS decays differ from those of an ideal experiment due to matter interactions, detector response and experimental misidentifications. We use the formal approach of Ref. [1] to relate the signal ratios of Eq. (4) to a prediction of the experimentally observed ratios:

$$R(t)^{\pm}_{\text{pred}} = R(t)^{\pm}(1 - \Delta_p^{\pm})(\epsilon_r)^{\pm 1} + p_{\text{other}}, \quad (5)$$

where the term $\epsilon_r \equiv \epsilon(K^+\pi^-)/\epsilon(K^-\pi^+)$ is the ratio of $K^{\pm}\pi^{\mp}$ detection efficiencies. The efficiencies related to the $\pi_s^{\pm}$ and $\mu^{\mp}$ candidates explicitly cancel in this ratio. The term $\Delta_p^{\pm}$ describes charge-specific peaking backgrounds produced by prompt charm mistakenly included in the DT sample, assumed to be zero after the "same-sign background subtraction" described in Sec. IV. The term p_{other} describes peaking backgrounds that contribute differently to RS and WS decays. All three of these terms are considered to be potentially time dependent.

III. DETECTOR AND TRIGGER

The LHCb detector [11,12] is a single-arm forward spectrometer covering the pseudorapidity range $2 < \eta < 5$, and is designed for the study of particles containing b or c quarks. The detector includes a high-precision tracking system consisting of a silicon-strip vertex detector surrounding the pp interaction region, a large-area silicon-strip detector located upstream of a dipole magnet with a bending power of about 4 Tm, and three stations of silicon-strip detectors and straw drift tubes placed downstream of the magnet. The tracking system provides a measurement of momentum, p, of charged particles with a fractional uncertainty that varies from 0.5% at 5 GeV/c to 1.0% at 200 GeV/c . The minimum distance of a track to a primary vertex (PV), the impact parameter (IP), is measured with a resolution of $(15 + 29/p_{\text{T}})$ μm, where p_{T} is the component of the momentum transverse to the beam, in GeV/c. Different types of charged hadrons are distinguished using information from two ring-imaging Cherenkov (RICH) detectors. Photons, electrons and hadrons are identified by a calorimeter system consisting of scintillating-pad and preshower detectors, an electromagnetic and a hadronic calorimeter. Muons are identified by a system composed of alternating layers of iron and multiwire proportional chambers.

The on-line candidate selection is performed by a trigger [13] which consists of a hardware stage, based on information from the calorimeter and muon systems, followed by a software stage. At the hardware stage, candidates are required to have a muon with $p_{\text{T}} > 1.64\,\text{GeV}/c$ (1.76 GeV/c) in the 2011 (2012) data sets. The software trigger, in which all charged particles with $p_{\text{T}} > 500(300)$ MeV/c are reconstructed for 2011 (2012) data, first requires a muon with $p_{\text{T}} > 1.0$ GeV/c, and a large χ^2_{IP}

with respect to any PV, where $\chi^2_{\rm IP}$ is defined as the difference in vertex fit χ^2 of a given PV reconstructed with and without the muon. Following this selection, the muon and at least one other final-state particle are required to be consistent with the topological signature of the decay of a b hadron [13]. To mitigate detector-related asymmetries, the magnet polarity is reversed periodically.

IV. OFF-LINE SELECTION

In the off-line selection, candidates must have a muon with $p > 3$ GeV/c, $p_{\rm T} > 1.2$ GeV/c and a track fit $\chi^2/{\rm ndf} < 4$, where ndf is the number of degrees of freedom in the fit. Each of the D^0 decay products and muon candidates must have $\chi^2_{\rm IP} > 9$, consistent with originating from a secondary vertex. The slow pion candidate must have $p > 2$ GeV/c and $p_{\rm T} > 300$ MeV/c, and have no associated hits in the muon stations. The combination of the K and π into a D^0 candidate must form a vertex that is well separated from the PV and have a χ^2 per degree of freedom less than 6. The D^0 candidate must also have $p_{\rm T} > 1.4$ GeV/c and its reconstructed invariant mass must lie within 24 MeV/c^2 of its measured mass [14]. The $D^{*+}\mu^-$ invariant mass must lie in the range 3.1–5.1 GeV/c^2. Candidates must satisfy a vertex fit which constrains the kaon and pion to come from the same vertex, and the muon, the slow pion and the D^0 candidate to come from a common vertex with a good $\chi^2/{\rm ndf}$. All final-state particles must pass stringent particle identification criteria from the RICH detectors, calorimeters and muon stations to improve the separation between signal and backgrounds produced by misidentified final-state particles. Candidates with reconstructed decay time $t/\tau < -0.5$ are vetoed, where τ is the measured D^0 lifetime [14] and t is calculated as $t = m_{D^0}L/p$, where L is the distance between the D^0 production and decay vertices, m_{D^0} is the observed candidate D^0 mass, and p is the D^0 momentum. The decay-time resolution is roughly 120 fs for the DT sample. Candidates which appear in both this data set and that of the earlier prompt analysis [1] are vetoed.

The same D^0 may appear in multiple candidate decay chains. In about 0.5% of cases, a single $D^0\mu^-$ combination has multiple slow pion candidates whose laboratory momentum vector directions lie within 0.6 mrad of each other. In such cases, we randomly accept one of the candidates and discard the others. When two slow pion candidates associated with a single $D^0\mu^-$ candidate are not collinear, the distributions of the $D^0\pi_s^+$ masses are consistent with the hypothesis that they (typically) result from candidates with a real D^{*+} decay plus an additional pion nearby in phase space. In such cases, we retain the multiple candidates; the fit described below correctly determines the signal and background rates as functions of $m(D^0\pi_s)$.

Real D^{*+} decays, produced either promptly or as decay products of b-hadron decays, can be mistakenly associated with muons not truly originating from b-hadron decays. In these cases, the production vertex of the D^0 may be wrongly determined. We remove these from the $D^0\pi_s^+$ distributions statistically by subtracting the corresponding $D^0\pi_s^+$ distributions of candidates where the D^{*+} and μ candidates have the same charge, the so-called same-sign samples. Signal candidates are referred to as the opposite-sign sample. The $m(D^0\pi_s^+)$ shapes to be subtracted are taken directly from the same-sign candidates, while otherwise satisfying all DT selection criteria. The absolute numbers of candidates are determined, in each bin of the D^0 decay time, by normalizing the same-sign rate to that of the opposite-sign DT sample in the $m(D^{*+}\mu^-)$ range 5.6–6 GeV/c^2, a region well above the masses of the B^0 and B_s^0 mesons and dominated by combinatorial backgrounds produced by false muon candidates. The ratio of same-sign to DT candidates in the signal region is roughly 1% and the ratio in the normalization region is 71%. A systematic uncertainty on the same-sign background subtraction is determined by setting the normalization factor to unity.

V. YIELD EXTRACTION AND FIT STRATEGY

Five bins of decay time are defined containing approximately equal numbers of RS decays. We determine D^{*+} signal yields using binned maximum likelihood fits to the $D^0\pi_s^+$ invariant mass distributions. The signal probability density function (PDF) consists of a sum of three Gaussian functions plus a Johnson S_U distribution [15] to model the asymmetric tails; the background PDFs are parametrized using empirical shapes of the form

$$(m(D^0\pi_s^+)/m_0 - 1)e^{c(m(D^0\pi_s^+)/m_0-1)}. \quad (6)$$

The parameter m_0 represents the kinematic limit of the distribution and is fixed to the sum of the measured mass of the pion and the D^0 [14]. The shapes of the RS and WS $D^{*\pm}$ are assumed to be the same and to be independent of the decay time. We first fit the time-integrated RS distribution to determine signal shape parameters. These are fixed for all subsequent fits. The background parameters vary independently in each fit. Systematic uncertainties related to this choice are assessed and discussed in Sec. VII. Figures 1(a) and 1(b) show the fits to the $D^0\pi_s^+$ time-integrated invariant mass distributions for RS and WS samples. They contain 1.73×10^6 and 6.68×10^3 D^{*+} decays, respectively.

The numbers of RS and WS signal candidates in each decay time bin are determined from fits, from which the observed WS to RS ratios are calculated. The term $p_{\rm other}$ is the ratio of the number of peaking events in the $m(D^0\pi_s^+)$

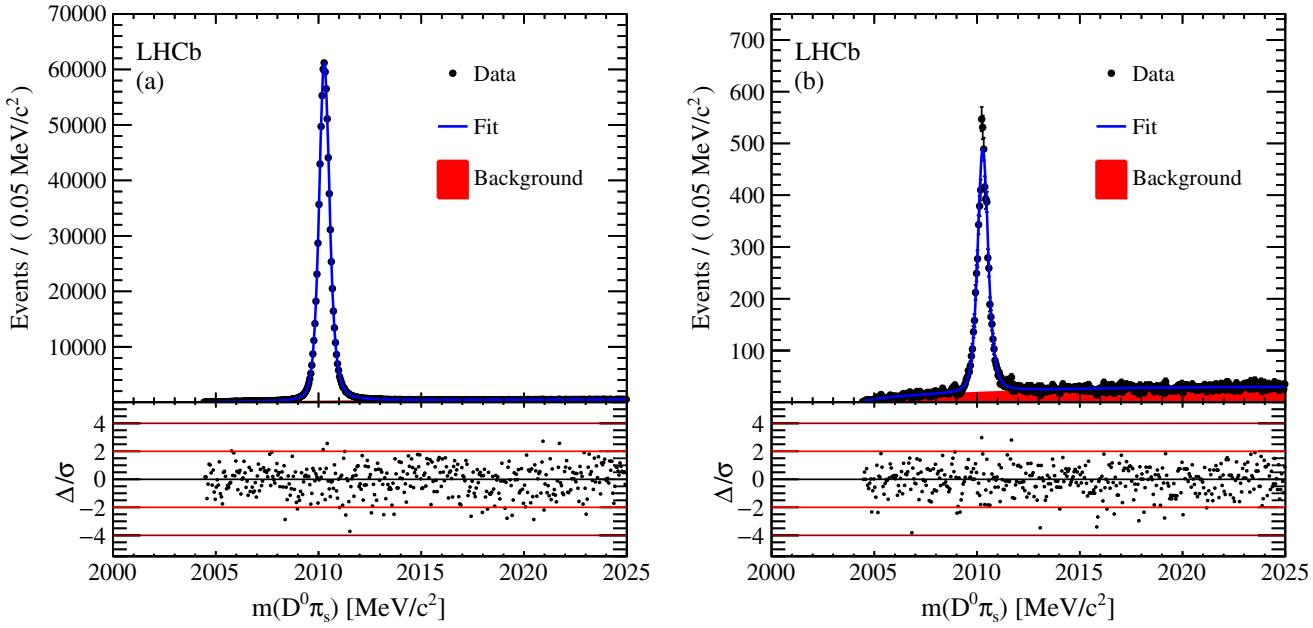

FIG. 1. The time-integrated $D^0\pi_s^+$ invariant mass distributions, after same-sign subtraction, for (a) RS decays and (b) WS decays. Fit projections are overlaid. Below each plot are the normalized residual distributions.

distribution from the D^0 sidebands of the WS sample projected into the signal region relative to the RS yield. We measure p_{other} to be $(7.4 \pm 1.8) \times 10^{-5}$. To measure the mixing and *CPV* parameters, the time dependence of these ratios is fit by minimizing

$$\chi^2 = \sum_i \left[\left(\frac{r_i^+ - \tilde{R}(t_i)^+}{\sigma_i^+} \right)^2 + \left(\frac{r_i^- - \tilde{R}(t_i)^-}{\sigma_i^-} \right)^2 \right] + \chi^2{}_\epsilon + \chi^2{}_{\text{peaking}} + \chi^2{}_{\text{other}}. \quad (7)$$

Here, $r_i^\pm$ is the measured $\text{WS}^\pm/\text{RS}^\pm$ ratio for either the $D^{*+}(D^0)$ or the $D^{*-}(\overline{D}^0)$ sample with error $\sigma_i^\pm$ in a decay time bin t_i and $\tilde{R}(t_i)$ is the value of $R(t)^\pm_{\text{pred}}$ averaged over the bin. The fit accounts for uncertainties in the relative $K^\pm\pi^\mp$ tracking and reconstruction efficiencies and rates of peaking backgrounds using Gaussian constraints ($\chi^2{}_\epsilon + \chi^2{}_{\text{peaking}} + \chi^2{}_{\text{other}}$). The term $\chi^2{}_{\text{other}}$ relating to the feedthrough of the prompt sample into the DT sample is explicitly zero in the DT analysis, but is needed for the simultaneous fit to the DT and prompt data sets. The statistical uncertainties reported by the fit therefore include the uncertainties associated with how precisely these factors are determined.

Three fits are performed using this framework. First, we fit the data assuming *CP* symmetry in the formalism of Eq. (4) [i.e. $R^+ = R^-$, $(x'^+)^2 = (x'^-)^2$ and $y'^+ = y'^-$]. Second, we fit the data requiring *CP* symmetry in the CF and DCS amplitudes (i.e. $R^+ = R^-$), but allow *CPV* in the mixing parameters themselves [$(x'^\pm)^2$ and $y'^\pm$]. Finally, we fit the data allowing all the parameters to float freely.

VI. RELATIVE EFFICIENCIES

The relative efficiency ϵ_r, used in Eq. (5), accounts for instrumental asymmetries in the $K^\mp\pi^\pm$ reconstruction efficiencies. The largest source of these is the difference between the inelastic cross sections of K^- and π^- mesons with matter, and those of their antiparticles. We measure ϵ_r, accounting for all detector effects as well as cross-section differences in a similar manner to the prompt analysis [1]. The efficiency is determined using the product of $D^+ \to K^-\pi^+\pi^+$ and $D^+ \to K^0_S(\to \pi^+\pi^-)\pi^+$ decay yields divided by the product of the corresponding charge-conjugate decay yields. The expected *CPV* associated with differing $K^0 \to K^0_S$ and $\overline{K}^0 \to K^0_S$ rates and the differences in neutral kaon inelastic cross sections with matter are accounted for [16]. Trigger and detection asymmetries associated with the muon candidates are calculated directly from data and included in the determination. The 1% asymmetry between D^+ and D^- production rates [17] cancels in this ratio, provided that the kinematic distributions are consistent across samples. To ensure this cancellation, we weight the $D^+ \to K^-\pi^+\pi^+$ candidates such that the kaon p_{T} and η and pion p_{T} distributions match those in the DT $K\pi$ sample. Similarly, $D^+ \to K^0_S\pi^+$ candidates are weighted by $D^+ p_{\text{T}}$ and η and pion p_{T} distributions to match those of the $D^+ \to K^-\pi^+\pi^+$. The weighting is performed using a gradient boosted decision tree implemented in SCIKIT-LEARN [18] accessed using the HEP_ML framework [19]. We measure the $K\pi$ detection asymmetry to be $A(K\pi) = (\epsilon_r - 1)/(\epsilon_r + 1) = (0.90 \pm 0.18 \pm 0.10)\%$ for the sample of this analysis, and find it to be independent of decay time.

TABLE I. Summary of systematic uncertainties for the DT analysis for each of the three fits described in the text.

Source of systematic uncertainty	Uncertainty on parameter					
	No CPV					
	$R_D[10^{-3}]$	$y'[10^{-3}]$	$x'^2[10^{-4}]$			
$D^{*+}\mu^+$ scaling	0.01	0.04	0.04			
$A(K\pi)$ time dependence	0.01	0.07	0.04			
RS fit model time variation	0.00	0.01	0.03			
No prompt veto	0.01	0.16	0.09			
Total	0.01	0.18	0.11			
	No direct CPV					
	$R_D[10^{-3}]$	$y'^+[10^{-3}]$	$(x'^+)^2[10^{-4}]$	$y'^-[10^{-3}]$	$(x'^-)^2[10^{-4}]$	
$D^{*+}\mu^+$ scaling	0.01	0.04	0.04	0.03	0.04	
$A(K\pi)$ time dependence	0.01	1.17	0.98	1.64	1.67	
RS fit model time variation	0.00	0.02	0.03	0.01	0.03	
No prompt veto	0.01	0.11	0.00	0.19	0.19	
Total	0.01	1.17	0.98	1.66	1.68	
	All CPV allowed					
	$R_D^+[10^{-3}]$	$y'^+[10^{-3}]$	$(x'^+)^2[10^{-4}]$	$R_D^-[10^{-3}]$	$y'^-[10^{-3}]$	$(x'^-)^2[10^{-4}]$
$D^{*+}\mu^+$ scaling	0.01	0.03	0.04	0.01	0.04	0.04
$A(K\pi)$ time dependence	0.06	0.25	0.03	0.07	0.28	0.03
RS fit model time variation	0.00	0.01	0.01	0.00	0.04	0.05
No prompt veto	0.01	0.09	0.01	0.01	0.21	0.19
Potential fit biases	0.00	0.18	0.30	0.00	0.18	0.33
Total	0.06	0.32	0.31	0.07	0.40	0.38

VII. SYSTEMATIC UNCERTAINTIES

The systematic uncertainties of the DT analysis are summarized in Table I. To avoid bias, offsets to each WS/RS ratio were randomly chosen to blind both direct and indirect CPV, as well as the central values of the mixing parameters. Cross-checks of the blinded data were performed by splitting the data into disjoint subsamples according to criteria that might be sensitive to systematic variations in detector response. We considered two subsamples of magnet polarity, integrated over the entire data taking period, two subsamples for the year in which the data was recorded, four subsamples splitting according to magnet polarity and year of data acquisition, three subsamples each of $K^\pm$ momentum, $\mu^\pm$ transverse momentum and $\pi^\pm$ transverse momentum. All observed variations in the fit results are consistent with being statistical fluctuations.

The ratio of RS D^{*-} to RS D^{*+} decays as a function of decay time is consistent with the hypothesis of decay-time independence with a p value of 0.06. We conservatively estimate a systematic uncertainty by modifying ϵ_r to allow for a linear time dependence that gives the best description of the RS data. As seen in Table I, this has essentially no effect on the results of the mixing fit where CP symmetry is assumed to be exact. It is the dominant systematic uncertainty in the fit requiring $R_D^+ = R_D^-$, and it produces a systematic uncertainty much smaller than the statistical error in the fit that allows all forms of CPV. Uncertainties are not symmetrized.

We determine systematic uncertainties related to variations of the fit procedure by considering alternative choices. To determine uncertainties related to subtraction of the same-sign background $m(D^0\pi_s)$ distributions from the opposite-sign ones, we subtract the raw same-sign distributions rather than the scaled distributions. To determine uncertainties related to excluding candidates considered in the prompt analysis [1] from the DT analysis, we repeat the DT analysis including those candidates. As an alternative to using a single signal shape at all decay times, we determine signal shapes using the RS signal in each decay time bin. We evaluate potential biases in fitting procedure by generating and fitting 11,000 simulated DT samples with values of x and y spanning the 2σ contour about the average values reported by HFAG [3]. The biases we observe are nonzero, and appear to be independent of the generated values. We assign a systematic uncertainty equal to the full observed bias. Table I summarizes the results of these studies. All systematic uncertainties are propagated to the final results using their full covariance matrices.

VIII. RESULTS

The efficiency-corrected and same-sign (SS) background subtracted WS/RS ratios of the DT data and the three fits described earlier are shown in Fig. 2. The fits are shown in a binned projection. The top two plots show the WS/RS ratio as a function of decay time for the candidates tagged at production as $D^0[R^+(t)]$ and as $\overline{D}^0[R^-(t)]$. Both sets of

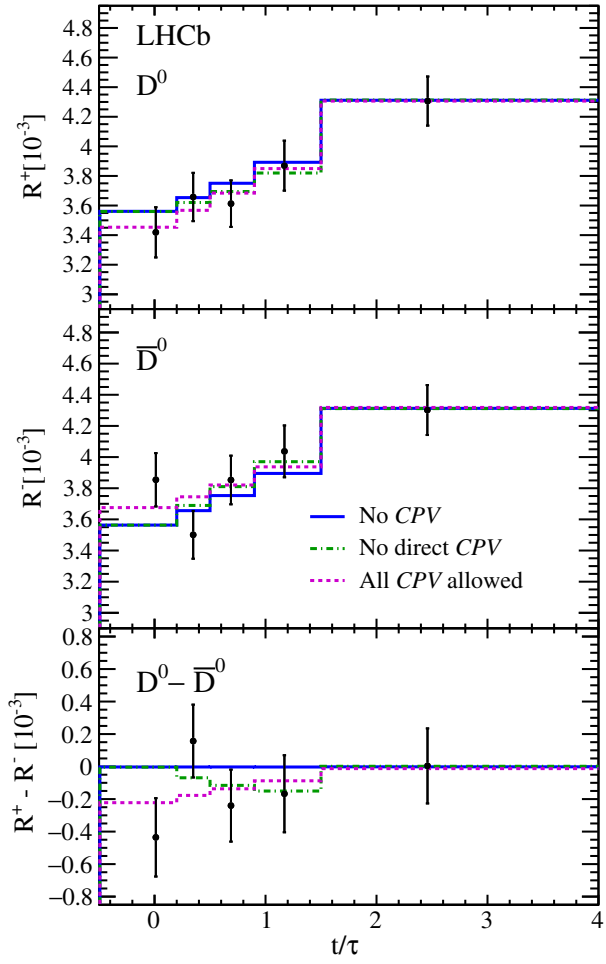

FIG. 2. Efficiency corrected and SS background subtracted ratios of WS/RS decays and fit projections for the DT sample. The top plot shows the D^0 ($R^+(t)$) sample. The middle plot shows the $\overline{D}^0$ ($R^-(t)$) sample. The bottom plot shows the difference between the top and middle plots. In all cases, the error bars superposed on the data points are those from the χ^2 minimization fits with no accounting for additional systematic uncertainties. The projections shown are for fits assuming *CP* symmetry (solid blue line), allowing no direct *CPV* (dashed-dotted green line), and allowing all forms of *CPV* (dashed magenta line). Bins are centered at the average value of t/τ of the bin.

points appear to lie on straight lines that intersect the vertical axis near 3.5×10^{-3} at $t/\tau = 0$ and rise approximately linearly to 4.3×10^{-3} near $t/\tau = 2.5$. The difference between the two ratios is shown in the bottom plot. The fit values for the parameters and their uncertainties are collected in Table II. The data are clearly consistent with the hypothesis of *CP* symmetry, i.e. that the two samples share exactly the same mixing parameters. If direct *CPV* is assumed to be zero ($R^+ = R^-$ at $t/\tau = 0$), as expected if tree-level amplitudes dominate the CF and DCS amplitudes, the difference in mixing rates (the slope) is observed to be very small. For this data set, the

TABLE II. Fitted parameters of the DT sample. The first uncertainties include the statistical uncertainty, as well as the peaking backgrounds and the $K\pi$ detection efficiency, and the second are systematic.

Parameter	Value		
	No *CPV*		
$R_D[10^{-3}]$	3.48	0.10	0.01
$x'^2[10^{-4}]$	0.28	3.10	0.11
$y'[10^{-3}]$	4.60	3.70	0.18
χ^2/ndf	6.3/7		
	No direct *CPV*		
$R_D[10^{-3}]$	3.48	0.10	0.01
$(x'^+)^2[10^{-4}]$	1.94	3.67	1.17
$y'^+[10^{-3}]$	2.79	4.27	0.98
$(x'^-)^2[10^{-4}]$	−1.53	4.04	1.68
$y'^-[10^{-3}]$	6.51	4.38	1.66
χ^2/ndf	5.6/5		
	All *CPV* allowed		
$R_D^+[10^{-3}]$	3.38	0.15	0.06
$(x'^+)^2[10^{-4}]$	−0.19	4.46	0.32
$y'^+[10^{-3}]$	5.81	5.25	0.31
$R_D^-[10^{-3}]$	3.60	0.15	0.07
$(x'^-)^2[10^{-4}]$	0.79	4.31	0.38
$y'^-[10^{-3}]$	3.32	5.21	0.40
χ^2/ndf	4.5/4		

statistical uncertainties are all much greater than the corresponding systematic uncertainties, which include the uncertainties from ϵ_r and peaking backgrounds. Correlation matrices between the fitted parameters are included in Appendix A, Tables V–VII.

The data of the prompt analysis [1], those of the DT analysis and the results of fitting the two (disjoint) samples simultaneously are shown in Fig. 3. The combined sets of data points in the top and middle plots lie on slightly curved lines that intersect the vertical axis near 3.4×10^{-3} at $t/\tau = 0$ and rise to approximately 5.9×10^{-3} just above $t/\tau = 6.0$. The samples are consistent with *CP* symmetry. The results of the simultaneous fit are reported in Table III. The corresponding results from the prompt analysis [1] are also reported in Table III for comparison. In Table III, the statistical and systematic uncertainties have been added in quadrature to allow direct comparison of the two sets of results. As all the systematic uncertainties for the prompt analysis were evaluated using χ^2 constraints as in Eq. (7), we determine systematic uncertainties for the simultaneous fits by repeating the fit variations as for the DT fit. These systematics are reported in Table IV. In general, the uncertainties from the combined fits are 10%–20% lower than those from the previous measurement [1]. The

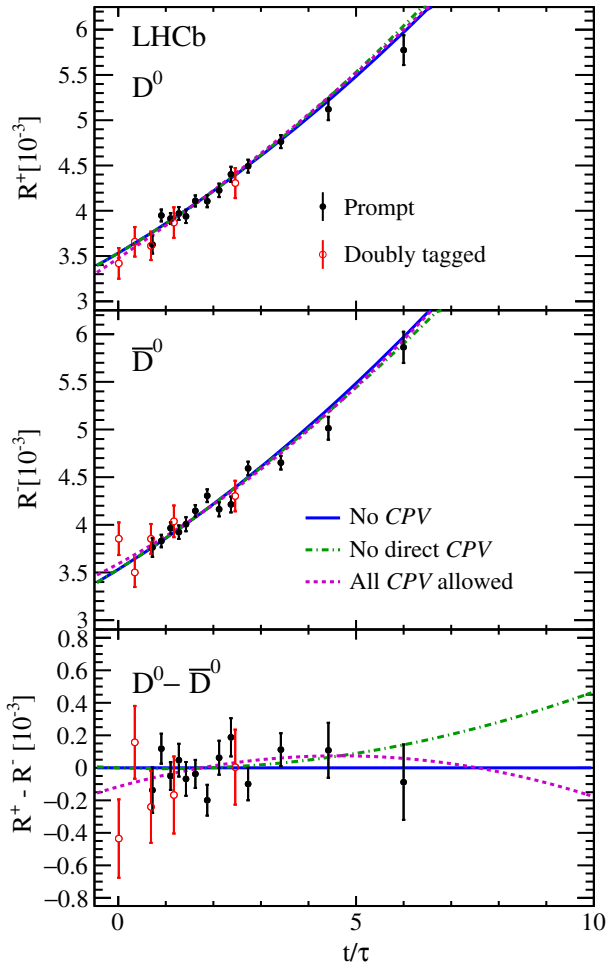

FIG. 3. Efficiency-corrected data and fit projections for the DT (red open circles) and prompt (black filled circles) samples. The top plot shows the D^0 ($R^+(t)$) samples. The middle plot shows the $\overline{D}^0$ ($R^-(t)$) samples. The bottom plot shows the difference between the top and middle plots. In all cases, the error bars superposed on the data points are those from the χ^2 minimization fits without accounting for additional systematic uncertainties. The projections shown are for fits assuming *CP* symmetry (solid blue line), allowing no direct *CPV* (dashed-dotted green line) and allowing all forms of *CPV* (dashed magenta line). Bins are centered at the average t/τ of the bin.

decrease in the uncertainty comes from the improved precision that the DT sample provides at low D^0 decay time. The corresponding correlation matrices are given in Appendix B, Tables VIII–X.

The combined fit of the DT and prompt sample is consistent with *CP* symmetry. The WS D^0 and $\overline{D}^0$ rates at $t/\tau = 0$ are equal within experimental uncertainties, indicating no direct *CP* violation. Similarly, the mixing rates are consistent within experimental uncertainties, as seen in the bottom plot of Fig. 3. In the combined fit of this analysis, assuming no direct *CP* violation, the difference between the projected WS/RS rates at $t/\tau = 6.0$ is only 0.15×10^{-3} (see the dashed-dotted line in the bottom plot of Fig. 3), where the WS/RS rates themselves have increased by about 2.5×10^{-3} (see the top and middle plots).

TABLE III. Simultaneous fit result of the DT and prompt samples. The prompt-only results from [1] are shown on the right for comparison. Statistical and systematic errors have been added in quadrature.

Parameter	DT + prompt	Prompt only
	No *CPV*	
$R_D[10^{-3}]$	3.533 ± 0.054	3.568 ± 0.067
$x'^2[10^{-4}]$	0.36 ± 0.43	0.55 ± 0.49
$y'[10^{-3}]$	5.23 ± 0.84	4.8 ± 0.9
χ^2/ndf	96.6/111	86.4/101
	No direct *CPV*	
$R_D[10^{-3}]$	3.533 ± 0.054	3.568 ± 0.067
$(x'^+)^2[10^{-4}]$	0.49 ± 0.50	0.64 ± 0.56
$y'^+[10^{-3}]$	5.14 ± 0.91	4.8 ± 1.1
$(x'^-)^2[10^{-4}]$	0.24 ± 0.50	0.46 ± 0.55
$y'^-[10^{-3}]$	5.32 ± 0.91	4.8 ± 1.1
χ^2/ndf	96.1/109	86.0/99
	All *CPV* allowed	
$R_D^+[10^{-3}]$	3.474 ± 0.081	3.545 ± 0.095
$(x'^+)^2[10^{-4}]$	0.11 ± 0.65	0.49 ± 0.70
$y'^+[10^{-3}]$	5.97 ± 1.25	5.1 ± 1.4
$R_D^-[10^{-3}]$	3.591 ± 0.081	3.591 ± 0.090
$(x'^-)^2[10^{-4}]$	0.61 ± 0.61	0.60 ± 0.68
$y'^-[10^{-3}]$	4.50 ± 1.21	4.5 ± 1.4
χ^2/ndf	95.0/108	85.9/98

The determination of the *CPV* parameters $|q/p|$ and φ from the difference in rates of WS D^0 and $\overline{D}^0$ requires the use of independent measurements, as these variables appear in the WS/RS ratios only in combination with the strong phase difference δ and with x and y, as seen in Eqs. (2) and (3). When the results are combined with independent measurements, as done by the Heavy Flavor Averaging Group [3], the precision of the constraints on $|q/p| - 1$ approximately scale with the precision of the difference in WS/RS ratios at high decay time divided by the average increase. Utilizing theoretical constraints such as Eq. (1), in addition to the experimental data, the precision on $|q/p|$ improves by about a factor of 4 [3].

IX. SUMMARY

In summary, the analysis of mixing and *CPV* parameters using the DT $D^0 \to K^{\mp}\pi^{\pm}$ samples provides results consistent with those of our earlier prompt analysis. Simultaneously fitting the disjoint data sets of the two analyses improves the precision of the measured parameters by 10%–20%, even though the DT analysis is based on

TABLE IV. Systematic uncertainties for the simultaneous fits of the DT and prompt data sets.

Systematic uncertainty	Uncertainty on parameter					
			No *CPV*			
	$R_D[10^{-3}]$	$y'[10^{-3}]$	$x'^2[10^{-4}]$			
$D^{*+}\mu^+$ scaling	0.00	0.05	0.02			
$A(K\pi)$ time dependence	0.00	0.02	0.01			
RS fit model time variation	0.00	0.00	0.00			
No prompt veto	0.00	0.04	0.02			
Total	0.01	0.07	0.03			
			No direct *CPV*			
	$R_D[10^{-3}]$	$y'^+[10^{-3}]$	$(x'^+)^2[10^{-4}]$	$y'^-[10^{-3}]$	$(x'^-)^2[10^{-4}]$	
$D^{*+}\mu^+$ scaling	0.00	0.05	0.02	0.05	0.02	
$A(K\pi)$ time dependence	0.00	0.02	0.02	0.06	0.03	
RS fit model time variation	0.00	0.00	0.00	0.00	0.00	
No prompt veto	0.00	0.04	0.02	0.04	0.02	
	0.01	0.07	0.03	0.09	0.05	
			All *CPV* allowed			
	$R_D^+[10^{-3}]$	$y'^+[10^{-3}]$	$(x'^+)^2[10^{-4}]$	$R_D^-[10^{-3}]$	$y'^-[10^{-3}]$	$(x'^-)^2[10^{-4}]$
$D^{*+}\mu^+$ scaling	0.00	0.06	0.02	0.00	0.05	0.02
$A(K\pi)$ time dependence	0.03	0.33	0.15	0.03	0.31	0.13
RS fit model time variation	0.00	0.00	0.00	0.00	0.01	0.00
No prompt veto	0.00	0.05	0.02	0.00	0.03	0.01
Total	0.03	0.34	0.15	0.03	0.31	0.13

almost 40 times fewer candidates than the prompt analysis. In part, this results from much cleaner signals in the DT analysis, and, in part, it results from the complementary higher acceptance of the DT trigger at low D decay times. The current results supersede those of our earlier publication [1].

ACKNOWLEDGMENTS

We express our gratitude to our colleagues in the CERN accelerator departments for the excellent performance of the LHC. We thank the technical and administrative staff at the LHCb institutes. We acknowledge support from CERN and from the national agencies: CAPES, CNPq, FAPERJ and FINEP (Brazil); NSFC (China); CNRS/IN2P3 (France); BMBF, DFG and MPG (Germany); INFN (Italy); FOM and NWO (Netherlands); MNiSW and NCN (Poland); MEN/IFA (Romania); MinES and FASO (Russia); MinECo (Spain); SNSF and SER (Switzerland); NASU (Ukraine); STFC (United Kingdom); and NSF (USA). We acknowledge the computing resources that are provided by CERN, IN2P3 (France), KIT and DESY (Germany), INFN (Italy), SURF (Netherlands), PIC (Spain), GridPP (United Kingdom), RRCKI and Yandex LLC (Russia), CSCS (Switzerland), IFIN-HH (Romania), CBPF (Brazil), PL-GRID (Poland) and OSC (USA). We are indebted to the communities behind the multiple open source software packages on which we depend. Individual groups or members have received support from AvH Foundation (Germany), EPLANET, Marie Skłodowska-Curie Actions and ERC (European Union), Conseil Général de Haute-Savoie, Labex ENIGMASS and OCEVU, Région Auvergne (France), RFBR and Yandex LLC (Russia), GVA, XuntaGal and GENCAT (Spain), Herchel Smith Fund, The Royal Society, Royal Commission for the Exhibition of 1851 and the Leverhulme Trust (United Kingdom).

APPENDIX A: CORRELATION MATRICES OF THE DT FIT

Below are included the correlation matrices for each of the fits to the DT sample. Table V shows the correlation matrices for the no CPV fit, Table VI shows the correlation matrix for the no direct CPV fit, and Table VII shows the correlation matrix for the all CPV allowed fit.

TABLE V. Correlation matrix for the no *CPV* fit to the DT data.

	R_D	y'	x'^2
R_D	1	−0.678	0.607
y'		1	−0.941
x'^2			1

TABLE VI. Correlation matrix for the no direct *CPV* fit to the DT data.

	R_D	y'^+	$(x'^+)^2$	y'^-	$(x'^-)^2$
R_D	1	−0.369	0.261	−0.374	0.309
y'^+		1	−0.944	0.448	−0.370
$(x'^+)^2$			1	−0.352	0.290
y'^-				1	−0.967
$(x'^-)^2$					1

TABLE VII. Correlation matrix for the all *CPV* allowed fit to the DT data.

	R_D^+	y'^+	$(x'^+)^2$	R_D^-	y'^-	$(x'^-)^2$
R_D^+	1	−0.658	0.043	−0.005	0.000	0.000
y'^+		1	0.438	−0.001	−0.000	−0.001
$(x'^+)^2$			1	−0.000	−0.000	−0.002
R_D^-				1	−0.621	0.074
y'^-					1	0.050
$(x'^-)^2$						1

APPENDIX B: CORRELATION MATRICES OF THE DT + PROMPT FIT

In this appendix, we include the correlation matrices for each of the simultaneous fits to the prompt + DT datasets. Table VIII shows the correlation matrix for the no CPV fit, Table IX shows the correlation matrix for the no direct CPV fit, and Table X shows the correlation matrix for the all CPV allowed fit.

TABLE VIII. Correlation matrix for the no *CPV* simultaneous fit to the prompt + DT data sets.

	R_D	y'	x'^2
R_D	1	−0.932	0.826
y'		1	−0.959
x'^2			1

TABLE IX. Correlation matrix for the no direct *CPV* simultaneous fit to the prompt + DT data sets.

	R_D	y'^+	$(x'^+)^2$	y'^-	$(x'^-)^2$
R_D	1	−0.854	0.686	−0.751	0.586
y'^+		1	−0.925	0.631	−0.501
$(x'^+)^2$			1	−0.563	0.458
y'^-				1	−0.937
$(x'^-)^2$					1

TABLE X. Correlation matrix for the all *CPV* allowed simultaneous fit to the prompt + DT data sets.

	R_D^+	y'^+	$(x'^+)^2$	R_D^-	y'^-	$(x'^-)^2$
R_D^+	1	−0.920	0.823	−0.007	−0.010	0.008
y'^+		1	−0.962	−0.011	0.000	−0.002
$(x'^+)^2$			1	0.009	−0.002	0.004
R_D^-				1	−0.918	0.812
y'^-					1	−0.956
$(x'^-)^2$						1

[1] R. Aaij *et al.* (LHCb Collaboration), Phys. Rev. Lett. **111**, 251801 (2013).
[2] Except when otherwise explicitly stated, charge-conjugate processes are implied.
[3] Y. Amhis *et al.* (Heavy Flavor Averaging Group Collaboration), arXiv:1412.7515; updated results and plots are available at http://www.slac.stanford.edu/xorg/hfag/ (November 11, 2016).
[4] L. Wolfenstein, Phys. Rev. Lett. **13**, 562 (1964).
[5] A. L. Kagan and M. D. Sokoloff, Phys. Rev. D **80**, 076008 (2009).
[6] A. F. Falk, Y. Grossman, Z. Ligeti, Y. Nir, and A. A. Petrov, Phys. Rev. D **69**, 114021 (2004).
[7] J. F. Donoghue, E. Golowich, B. R. Holstein, and J. Trampetić, Phys. Rev. D **33**, 179 (1986).
[8] A. F. Falk, Y. Grossman, Z. Ligeti, and A. A. Petrov, Phys. Rev. D **65**, 054034 (2002).
[9] S. Bianco, F. L. Fabbri, D. Benson, and I. Bigi, Riv. Nuovo Cimento Soc. Ital. Fis. **26N7**, 1 (2003).
[10] G. Burdman and I. Shipsey, Annu. Rev. Nucl. Part. Sci. **53**, 431 (2003).
[11] A. A. Alves, Jr. *et al.* (LHCb Collaboration), J. Instrum. **3**, S08005 (2008).
[12] R. Aaij *et al.* (LHCb Collaboration), Int. J. Mod. Phys. A **30**, 1530022 (2015).
[13] R. Aaij *et al.*, J. Instrum. **8**, P04022 (2013).
[14] K. A. Olive *et al.* (Particle Data Group Collaboration), Chin. Phys. C **38**, 090001 (2014), and 2015 update.
[15] N. L. Johnson, Biometrika **36**, 149 (1949).
[16] R. Aaij *et al.* (LHCb Collaboration), J. High Energy Phys. 07 (2014) 041.
[17] R. Aaij *et al.* (LHCb Collaboration), Phys. Lett. B **718**, 902 (2013).
[18] F. Pedregosa *et al.*, J. Mach. Learn. Res. **12**, 2825 (2011).
[19] A. Rogozhnikov *et al.*, HEP_ML, https://arogozhnikov.github.io/hep_ml/.

R. Aaij,[40] B. Adeva,[39] M. Adinolfi,[48] Z. Ajaltouni,[5] S. Akar,[6] J. Albrecht,[10] F. Alessio,[40] M. Alexander,[53] S. Ali,[43] G. Alkhazov,[31] P. Alvarez Cartelle,[55] A. A. Alves Jr.,[59] S. Amato,[2] S. Amerio,[23] Y. Amhis,[7] L. An,[41] L. Anderlini,[18] G. Andreassi,[41] M. Andreotti,[17,g] J. E. Andrews,[60] R. B. Appleby,[56] F. Archilli,[43] P. d'Argent,[12] J. Arnau Romeu,[6] A. Artamonov,[37] M. Artuso,[61] E. Aslanides,[6] G. Auriemma,[26] M. Baalouch,[5] I. Babuschkin,[56] S. Bachmann,[12] J. J. Back,[50] A. Badalov,[38] C. Baesso,[62] S. Baker,[55] W. Baldini,[17] R. J. Barlow,[56] C. Barschel,[40] S. Barsuk,[7] W. Barter,[40] M. Baszczyk,[27] V. Batozskaya,[29] B. Batsukh,[61] V. Battista,[41] A. Bay,[41] L. Beaucourt,[4] J. Beddow,[53] F. Bedeschi,[24] I. Bediaga,[1] L. J. Bel,[43] V. Bellee,[41] N. Belloli,[21,i] K. Belous,[37] I. Belyaev,[32] E. Ben-Haim,[8] G. Bencivenni,[19] S. Benson,[43] J. Benton,[48] A. Berezhnoy,[33] R. Bernet,[42] A. Bertolin,[23] F. Betti,[15] M.-O. Bettler,[40] M. van Beuzekom,[43] Ia. Bezshyiko,[42] S. Bifani,[47] P. Billoir,[8] T. Bird,[56] A. Birnkraut,[10] A. Bitadze,[56] A. Bizzeti,[18,u] T. Blake,[50] F. Blanc,[41] J. Blouw,[11,†] S. Blusk,[61] V. Bocci,[26] T. Boettcher,[58] A. Bondar,[36,w] N. Bondar,[31,40] W. Bonivento,[16] A. Borgheresi,[21,i] S. Borghi,[56] M. Borisyak,[35] M. Borsato,[39] F. Bossu,[7] M. Boubdir,[9] T. J. V. Bowcock,[54] E. Bowen,[42] C. Bozzi,[17,40] S. Braun,[12] M. Britsch,[12] T. Britton,[61] J. Brodzicka,[56] E. Buchanan,[48] C. Burr,[56] A. Bursche,[2] J. Buytaert,[40] S. Cadeddu,[16] R. Calabrese,[17,g] M. Calvi,[21,i] M. Calvo Gomez,[38,m] A. Camboni,[38] P. Campana,[19] D. Campora Perez,[40] D. H. Campora Perez,[40] L. Capriotti,[56] A. Carbone,[15,e] G. Carboni,[25,j] R. Cardinale,[20,h] A. Cardini,[16] P. Carniti,[21,i] L. Carson,[52] K. Carvalho Akiba,[2] G. Casse,[54] L. Cassina,[21,i] L. Castillo Garcia,[41] M. Cattaneo,[40] Ch. Cauet,[10] G. Cavallero,[20] R. Cenci,[24,t] M. Charles,[8] Ph. Charpentier,[40] G. Chatzikonstantinidis,[47] M. Chefdeville,[4] S. Chen,[56] S.-F. Cheung,[57] V. Chobanova,[39] M. Chrzaszcz,[42,27] X. Cid Vidal,[39] G. Ciezarek,[43] P. E. L. Clarke,[52] M. Clemencic,[40] H. V. Cliff,[49] J. Closier,[40] V. Coco,[59] J. Cogan,[6] E. Cogneras,[5] V. Cogoni,[16,40,f] L. Cojocariu,[30] G. Collazuol,[23,o] P. Collins,[40] A. Comerma-Montells,[12] A. Contu,[40] A. Cook,[48] G. Coombs,[40] S. Coquereau,[38] G. Corti,[40] M. Corvo,[17,g] C. M. Costa Sobral,[50] B. Couturier,[40] G. A. Cowan,[52] D. C. Craik,[52] A. Crocombe,[50] M. Cruz Torres,[62] S. Cunliffe,[55] R. Currie,[55] C. D'Ambrosio,[40] F. Da Cunha Marinho,[2] E. Dall'Occo,[43] J. Dalseno,[48] P. N. Y. David,[43] A. Davis,[59] O. De Aguiar Francisco,[2] K. De Bruyn,[6] S. De Capua,[56] M. De Cian,[12] J. M. De Miranda,[1] L. De Paula,[2] M. De Serio,[14,d] P. De Simone,[19] C.-T. Dean,[53] D. Decamp,[4] M. Deckenhoff,[10] L. Del Buono,[8] M. Demmer,[10] D. Derkach,[35] O. Deschamps,[5] F. Dettori,[40] B. Dey,[22] A. Di Canto,[40] H. Dijkstra,[40] F. Dordei,[40] M. Dorigo,[41] A. Dosil Suárez,[39] A. Dovbnya,[45] K. Dreimanis,[54] L. Dufour,[43] G. Dujany,[56] K. Dungs,[40] P. Durante,[40] R. Dzhelyadin,[37] A. Dziurda,[40] A. Dzyuba,[31] N. Déléage,[4] S. Easo,[51] M. Ebert,[52] U. Egede,[55] V. Egorychev,[32] S. Eidelman,[36,w] S. Eisenhardt,[52] U. Eitschberger,[10] R. Ekelhof,[10] L. Eklund,[53] Ch. Elsasser,[42] S. Ely,[61] S. Esen,[12] H. M. Evans,[49] T. Evans,[57] A. Falabella,[15] N. Farley,[47] S. Farry,[54] R. Fay,[54] D. Fazzini,[21,i] D. Ferguson,[52] V. Fernandez Albor,[39] A. Fernandez Prieto,[39] F. Ferrari,[15,40] F. Ferreira Rodrigues,[1] M. Ferro-Luzzi,[40] S. Filippov,[34] R. A. Fini,[14] M. Fiore,[17,g] M. Fiorini,[17,g] M. Firlej,[28] C. Fitzpatrick,[41] T. Fiutowski,[28] F. Fleuret,[7,b] K. Fohl,[40] M. Fontana,[16,40] F. Fontanelli,[20,h] D. C. Forshaw,[61] R. Forty,[40] V. Franco Lima,[54] M. Frank,[40] C. Frei,[40] J. Fu,[22,q] E. Furfaro,[25,j] C. Färber,[40]

A. Gallas Torreira,[39] D. Galli,[15,e] S. Gallorini,[23] S. Gambetta,[52] M. Gandelman,[2] P. Gandini,[57] Y. Gao,[3] L. M. Garcia Martin,[68] J. García Pardiñas,[39] J. Garra Tico,[49] L. Garrido,[38] P. J. Garsed,[49] D. Gascon,[38] C. Gaspar,[40] L. Gavardi,[10] G. Gazzoni,[5] D. Gerick,[12] E. Gersabeck,[12] M. Gersabeck,[56] T. Gershon,[50] Ph. Ghez,[4] S. Gianì,[41] V. Gibson,[49] O. G. Girard,[41] L. Giubega,[30] K. Gizdov,[52] V. V. Gligorov,[8] D. Golubkov,[32] A. Golutvin,[55,40] A. Gomes,[1,a] I. V. Gorelov,[33] C. Gotti,[21,i] M. Grabalosa Gándara,[5] R. Graciani Diaz,[38] L. A. Granado Cardoso,[40] E. Graugés,[38] E. Graverini,[42] G. Graziani,[18] A. Grecu,[30] P. Griffith,[47] L. Grillo,[21,40,i] B. R. Gruberg Cazon,[57] O. Grünberg,[66] E. Gushchin,[34] Yu. Guz,[37] T. Gys,[40] C. Göbel,[62] T. Hadavizadeh,[57] C. Hadjivasiliou,[5] G. Haefeli,[41] C. Haen,[40] S. C. Haines,[49] S. Hall,[55] B. Hamilton,[60] X. Han,[12] S. Hansmann-Menzemer,[12] N. Harnew,[57] S. T. Harnew,[48] J. Harrison,[56] M. Hatch,[40] J. He,[63] T. Head,[41] A. Heister,[9] K. Hennessy,[54] P. Henrard,[5] L. Henry,[8] J. A. Hernando Morata,[39] E. van Herwijnen,[40] M. Heß,[66] A. Hicheur,[2] D. Hill,[57] C. Hombach,[56] H. Hopchev,[41] W. Hulsbergen,[43] T. Humair,[55] M. Hushchyn,[35] N. Hussain,[57] D. Hutchcroft,[54] M. Idzik,[28] P. Ilten,[58] R. Jacobsson,[40] A. Jaeger,[12] J. Jalocha,[57] E. Jans,[43] A. Jawahery,[60] F. Jiang,[3] M. John,[57] D. Johnson,[40] C. R. Jones,[49] C. Joram,[40] B. Jost,[40] N. Jurik,[61] S. Kandybei,[45] W. Kanso,[6] M. Karacson,[40] J. M. Kariuki,[48] S. Karodia,[53] M. Kecke,[12] M. Kelsey,[61] I. R. Kenyon,[47] M. Kenzie,[49] T. Ketel,[44] E. Khairullin,[35] B. Khanji,[21,40,i] C. Khurewathanakul,[41] T. Kirn,[9] S. Klaver,[56] K. Klimaszewski,[29] S. Koliiev,[46] M. Kolpin,[12] I. Komarov,[41] R. F. Koopman,[44] P. Koppenburg,[43] A. Kosmyntseva,[32] A. Kozachuk,[33] M. Kozeiha,[5] L. Kravchuk,[34] K. Kreplin,[12] M. Kreps,[50] P. Krokovny,[36,w] F. Kruse,[10] W. Krzemien,[29] W. Kucewicz,[27,l] M. Kucharczyk,[27] V. Kudryavtsev,[36,w] A. K. Kuonen,[41] K. Kurek,[29] T. Kvaratskheliya,[32,40] D. Lacarrere,[40] G. Lafferty,[56] A. Lai,[16] D. Lambert,[52] G. Lanfranchi,[19] C. Langenbruch,[9] T. Latham,[50] C. Lazzeroni,[47] R. Le Gac,[6] J. van Leerdam,[43] J.-P. Lees,[4] A. Leflat,[33,40] J. Lefrançois,[7] R. Lefèvre,[5] F. Lemaitre,[40] E. Lemos Cid,[39] O. Leroy,[6] T. Lesiak,[27] B. Leverington,[12] Y. Li,[7] T. Likhomanenko,[35,67] R. Lindner,[40] C. Linn,[40] F. Lionetto,[42] B. Liu,[16] X. Liu,[3] D. Loh,[50] I. Longstaff,[53] J. H. Lopes,[2] D. Lucchesi,[23,o] M. Lucio Martinez,[39] H. Luo,[52] A. Lupato,[23] E. Luppi,[17,g] O. Lupton,[57] A. Lusiani,[24] X. Lyu,[63] F. Machefert,[7] F. Maciuc,[30] O. Maev,[31] K. Maguire,[56] S. Malde,[57] A. Malinin,[67] T. Maltsev,[36] G. Manca,[7] G. Mancinelli,[6] P. Manning,[61] J. Maratas,[5,v] J. F. Marchand,[4] U. Marconi,[15] C. Marin Benito,[38] P. Marino,[24,t] J. Marks,[12] G. Martellotti,[26] M. Martin,[6] M. Martinelli,[41] D. Martinez Santos,[39] F. Martinez Vidal,[68] D. Martins Tostes,[2] L. M. Massacrier,[7] A. Massafferri,[1] R. Matev,[40] A. Mathad,[50] Z. Mathe,[40] C. Matteuzzi,[21] A. Mauri,[42] B. Maurin,[41] A. Mazurov,[47] M. McCann,[55] J. McCarthy,[47] A. McNab,[56] R. McNulty,[13] B. Meadows,[59] F. Meier,[10] M. Meissner,[12] D. Melnychuk,[29] M. Merk,[43] A. Merli,[22,q] E. Michielin,[23] D. A. Milanes,[65] M.-N. Minard,[4] D. S. Mitzel,[12] A. Mogini,[8] J. Molina Rodriguez,[62] I. A. Monroy,[65] S. Monteil,[5] M. Morandin,[23] P. Morawski,[28] A. Mordà,[6] M. J. Morello,[24,t] J. Moron,[28] A. B. Morris,[52] R. Mountain,[61] F. Muheim,[52] M. Mulder,[43] M. Mussini,[15] D. Müller,[56] J. Müller,[10] K. Müller,[42] V. Müller,[10] P. Naik,[48] T. Nakada,[41] R. Nandakumar,[51] A. Nandi,[57] I. Nasteva,[2] M. Needham,[52] N. Neri,[22] S. Neubert,[12] N. Neufeld,[40] M. Neuner,[12] A. D. Nguyen,[41] C. Nguyen-Mau,[41,n] S. Nieswand,[9] R. Niet,[10] N. Nikitin,[33] T. Nikodem,[12] A. Novoselov,[37] D. P. O'Hanlon,[50] A. Oblakowska-Mucha,[28] V. Obraztsov,[37] S. Ogilvy,[19] R. Oldeman,[49] C. J. G. Onderwater,[69] J. M. Otalora Goicochea,[2] A. Otto,[40] P. Owen,[42] A. Oyanguren,[68] P. R. Pais,[41] A. Palano,[14,d] F. Palombo,[22,q] M. Palutan,[19] J. Panman,[40] A. Papanestis,[51] M. Pappagallo,[14,d] L. L. Pappalardo,[17,g] W. Parker,[60] C. Parkes,[56] G. Passaleva,[18] A. Pastore,[14,d] G. D. Patel,[54] M. Patel,[55] C. Patrignani,[15,e] A. Pearce,[56,51] A. Pellegrino,[43] G. Penso,[26] M. Pepe Altarelli,[40] S. Perazzini,[40] P. Perret,[5] L. Pescatore,[47] K. Petridis,[48] A. Petrolini,[20,h] A. Petrov,[67] M. Petruzzo,[22,q] E. Picatoste Olloqui,[38] B. Pietrzyk,[4] M. Pikies,[27] D. Pinci,[26] A. Pistone,[20] A. Piucci,[12] S. Playfer,[52] M. Plo Casasus,[39] T. Poikela,[40] F. Polci,[8] A. Poluektov,[50,36] I. Polyakov,[61] E. Polycarpo,[2] G. J. Pomery,[48] A. Popov,[37] D. Popov,[11,40] B. Popovici,[30] S. Poslavskii,[37] C. Potterat,[2] E. Price,[48] J. D. Price,[54] J. Prisciandaro,[39] A. Pritchard,[54] C. Prouve,[48] V. Pugatch,[46] A. Puig Navarro,[41] G. Punzi,[24,p] W. Qian,[57] R. Quagliani,[7,48] B. Rachwal,[27] J. H. Rademacker,[48] M. Rama,[24] M. Ramos Pernas,[39] M. S. Rangel,[2] I. Raniuk,[45] G. Raven,[44] F. Redi,[55] S. Reichert,[10] A. C. dos Reis,[1] C. Remon Alepuz,[68] V. Renaudin,[7] S. Ricciardi,[51] S. Richards,[48] M. Rihl,[40] K. Rinnert,[54] V. Rives Molina,[38] P. Robbe,[7,40] A. B. Rodrigues,[1] E. Rodrigues,[59] J. A. Rodriguez Lopez,[65] P. Rodriguez Perez,[56,†] A. Rogozhnikov,[35] S. Roiser,[40] A. Rollings,[57] V. Romanovskiy,[37] A. Romero Vidal,[39] J. W. Ronayne,[13] M. Rotondo,[19] M. S. Rudolph,[61] T. Ruf,[40] P. Ruiz Valls,[68] J. J. Saborido Silva,[39] E. Sadykhov,[32] N. Sagidova,[31] B. Saitta,[16,f] V. Salustino Guimaraes,[2] C. Sanchez Mayordomo,[68] B. Sanmartin Sedes,[39] R. Santacesaria,[26] C. Santamarina Rios,[39] M. Santimaria,[19] E. Santovetti,[25,j] A. Sarti,[19,k] C. Satriano,[26,s] A. Satta,[25] D. M. Saunders,[48] D. Savrina,[32,33] S. Schael,[9] M. Schellenberg,[10] M. Schiller,[40] H. Schindler,[40] M. Schlupp,[10] M. Schmelling,[11] T. Schmelzer,[10] B. Schmidt,[40] O. Schneider,[41] A. Schopper,[40] K. Schubert,[10] M. Schubiger,[41] M.-H. Schune,[7] R. Schwemmer,[40] B. Sciascia,[19] A. Sciubba,[26,k] A. Semennikov,[32] A. Sergi,[47] N. Serra,[42] J. Serrano,[6] L. Sestini,[23] P. Seyfert,[21] M. Shapkin,[37] I. Shapoval,[45] Y. Shcheglov,[31] T. Shears,[54]

L. Shekhtman,[36,w] V. Shevchenko,[67] A. Shires,[10] B. G. Siddi,[17,40] R. Silva Coutinho,[42] L. Silva de Oliveira,[2] G. Simi,[23,o] S. Simone,[14,d] M. Sirendi,[49] N. Skidmore,[48] T. Skwarnicki,[61] E. Smith,[55] I. T. Smith,[52] J. Smith,[49] M. Smith,[55] H. Snoek,[43] M. D. Sokoloff,[59] F. J. P. Soler,[53] B. Souza De Paula,[2] B. Spaan,[10] P. Spradlin,[53] S. Sridharan,[40] F. Stagni,[40] M. Stahl,[12] S. Stahl,[40] P. Stefko,[41] S. Stefkova,[55] O. Steinkamp,[42] S. Stemmle,[12] O. Stenyakin,[37] S. Stevenson,[57] S. Stoica,[30] S. Stone,[61] B. Storaci,[42] S. Stracka,[24,p] M. Straticiuc,[30] U. Straumann,[42] L. Sun,[59] W. Sutcliffe,[55] K. Swientek,[28] V. Syropoulos,[44] M. Szczekowski,[29] T. Szumlak,[28] S. T'Jampens,[4] A. Tayduganov,[6] T. Tekampe,[10] M. Teklishyn,[7] G. Tellarini,[17,g] F. Teubert,[40] E. Thomas,[40] J. van Tilburg,[43] M. J. Tilley,[55] V. Tisserand,[4] M. Tobin,[41] S. Tolk,[49] L. Tomassetti,[17,g] D. Tonelli,[40] S. Topp-Joergensen,[57] F. Toriello,[61] E. Tournefier,[4] S. Tourneur,[41] K. Trabelsi,[41] M. Traill,[53] M. T. Tran,[41] M. Tresch,[42] A. Trisovic,[40] A. Tsaregorodtsev,[6] P. Tsopelas,[43] A. Tully,[49] N. Tuning,[43] A. Ukleja,[29] A. Ustyuzhanin,[35] U. Uwer,[12] C. Vacca,[16,f] V. Vagnoni,[15,40] A. Valassi,[40] S. Valat,[40] G. Valenti,[15] A. Vallier,[7] R. Vazquez Gomez,[19] P. Vazquez Regueiro,[39] S. Vecchi,[17] M. van Veghel,[43] J. J. Velthuis,[48] M. Veltri,[18,r] G. Veneziano,[41] A. Venkateswaran,[61] M. Vernet,[5] M. Vesterinen,[12] B. Viaud,[7] D. Vieira,[1] M. Vieites Diaz,[39] X. Vilasis-Cardona,[38,m] V. Volkov,[33] A. Vollhardt,[42] B. Voneki,[40] A. Vorobyev,[31] V. Vorobyev,[36,w] C. Voß,[66] J. A. de Vries,[43] C. Vázquez Sierra,[39] R. Waldi,[66] C. Wallace,[50] R. Wallace,[13] J. Walsh,[24] J. Wang,[61] D. R. Ward,[49] H. M. Wark,[54] N. K. Watson,[47] D. Websdale,[55] A. Weiden,[42] M. Whitehead,[40] J. Wicht,[50] G. Wilkinson,[57,40] M. Wilkinson,[61] M. Williams,[40] M. P. Williams,[47] M. Williams,[58] T. Williams,[47] F. F. Wilson,[51] J. Wimberley,[60] J. Wishahi,[10] W. Wislicki,[29] M. Witek,[27] G. Wormser,[7] S. A. Wotton,[49] K. Wraight,[53] S. Wright,[49] K. Wyllie,[40] Y. Xie,[64] Z. Xing,[61] Z. Xu,[41] Z. Yang,[3] H. Yin,[64] J. Yu,[64] X. Yuan,[36,w] O. Yushchenko,[37] K. A. Zarebski,[47] M. Zavertyaev,[11,c] L. Zhang,[3] Y. Zhang,[7] Y. Zhang,[63] A. Zhelezov,[12] Y. Zheng,[63] A. Zhokhov,[32] X. Zhu,[3] V. Zhukov,[9] and S. Zucchelli[15]

(LHCb Collaboration)

[1]*Centro Brasileiro de Pesquisas Físicas (CBPF), Rio de Janeiro, Brazil*
[2]*Universidade Federal do Rio de Janeiro (UFRJ), Rio de Janeiro, Brazil*
[3]*Center for High Energy Physics, Tsinghua University, Beijing, China*
[4]*LAPP, Université Savoie Mont-Blanc, CNRS/IN2P3, Annecy-Le-Vieux, France*
[5]*Clermont Université, Université Blaise Pascal, CNRS/IN2P3, LPC, Clermont-Ferrand, France*
[6]*CPPM, Aix-Marseille Université, CNRS/IN2P3, Marseille, France*
[7]*LAL, Université Paris-Sud, CNRS/IN2P3, Orsay, France*
[8]*LPNHE, Université Pierre et Marie Curie, Université Paris Diderot, CNRS/IN2P3, Paris, France*
[9]*I. Physikalisches Institut, RWTH Aachen University, Aachen, Germany*
[10]*Fakultät Physik, Technische Universität Dortmund, Dortmund, Germany*
[11]*Max-Planck-Institut für Kernphysik (MPIK), Heidelberg, Germany*
[12]*Physikalisches Institut, Ruprecht-Karls-Universität Heidelberg, Heidelberg, Germany*
[13]*School of Physics, University College Dublin, Dublin, Ireland*
[14]*Sezione INFN di Bari, Bari, Italy*
[15]*Sezione INFN di Bologna, Bologna, Italy*
[16]*Sezione INFN di Cagliari, Cagliari, Italy*
[17]*Sezione INFN di Ferrara, Ferrara, Italy*
[18]*Sezione INFN di Firenze, Firenze, Italy*
[19]*Laboratori Nazionali dell'INFN di Frascati, Frascati, Italy*
[20]*Sezione INFN di Genova, Genova, Italy*
[21]*Sezione INFN di Milano Bicocca, Milano, Italy*
[22]*Sezione INFN di Milano, Milano, Italy*
[23]*Sezione INFN di Padova, Padova, Italy*
[24]*Sezione INFN di Pisa, Pisa, Italy*
[25]*Sezione INFN di Roma Tor Vergata, Roma, Italy*
[26]*Sezione INFN di Roma La Sapienza, Roma, Italy*
[27]*Henryk Niewodniczanski Institute of Nuclear Physics Polish Academy of Sciences, Kraków, Poland*
[28]*AGH - University of Science and Technology, Faculty of Physics and Applied Computer Science, Kraków, Poland*
[29]*National Center for Nuclear Research (NCBJ), Warsaw, Poland*
[30]*Horia Hulubei National Institute of Physics and Nuclear Engineering, Bucharest-Magurele, Romania*
[31]*Petersburg Nuclear Physics Institute (PNPI), Gatchina, Russia*
[32]*Institute of Theoretical and Experimental Physics (ITEP), Moscow, Russia*

[33]*Institute of Nuclear Physics, Moscow State University (SINP MSU), Moscow, Russia*
[34]*Institute for Nuclear Research of the Russian Academy of Sciences (INR RAN), Moscow, Russia*
[35]*Yandex School of Data Analysis, Moscow, Russia*
[36]*Budker Institute of Nuclear Physics (SB RAS), Novosibirsk, Russia*
[37]*Institute for High Energy Physics (IHEP), Protvino, Russia*
[38]*ICCUB, Universitat de Barcelona, Barcelona, Spain*
[39]*Universidad de Santiago de Compostela, Santiago de Compostela, Spain*
[40]*European Organization for Nuclear Research (CERN), Geneva, Switzerland*
[41]*Ecole Polytechnique Fédérale de Lausanne (EPFL), Lausanne, Switzerland*
[42]*Physik-Institut, Universität Zürich, Zürich, Switzerland*
[43]*Nikhef National Institute for Subatomic Physics, Amsterdam, Netherlands*
[44]*Nikhef National Institute for Subatomic Physics and VU University Amsterdam, Amsterdam, Netherlands*
[45]*NSC Kharkiv Institute of Physics and Technology (NSC KIPT), Kharkiv, Ukraine*
[46]*Institute for Nuclear Research of the National Academy of Sciences (KINR), Kyiv, Ukraine*
[47]*University of Birmingham, Birmingham, United Kingdom*
[48]*H.H. Wills Physics Laboratory, University of Bristol, Bristol, United Kingdom*
[49]*Cavendish Laboratory, University of Cambridge, Cambridge, United Kingdom*
[50]*Department of Physics, University of Warwick, Coventry, United Kingdom*
[51]*STFC Rutherford Appleton Laboratory, Didcot, United Kingdom*
[52]*School of Physics and Astronomy, University of Edinburgh, Edinburgh, United Kingdom*
[53]*School of Physics and Astronomy, University of Glasgow, Glasgow, United Kingdom*
[54]*Oliver Lodge Laboratory, University of Liverpool, Liverpool, United Kingdom*
[55]*Imperial College London, London, United Kingdom*
[56]*School of Physics and Astronomy, University of Manchester, Manchester, United Kingdom*
[57]*Department of Physics, University of Oxford, Oxford, United Kingdom*
[58]*Massachusetts Institute of Technology, Cambridge, Massachusetts, USA*
[59]*University of Cincinnati, Cincinnati, Ohio, USA*
[60]*University of Maryland, College Park, Maryland, USA*
[61]*Syracuse University, Syracuse, New York, USA*
[62]*Pontifícia Universidade Católica do Rio de Janeiro (PUC-Rio), Rio de Janeiro, Brazil (associated with Universidade Federal do Rio de Janeiro (UFRJ), Rio de Janeiro, Brazil)*
[63]*University of Chinese Academy of Sciences, Beijing, China (associated with Center for High Energy Physics, Tsinghua University, Beijing, China)*
[64]*Institute of Particle Physics, Central China Normal University, Wuhan, Hubei, China (associated with Center for High Energy Physics, Tsinghua University, Beijing, China)*
[65]*Departamento de Fisica , Universidad Nacional de Colombia, Bogota, Colombia (associated with LPNHE, Université Pierre et Marie Curie, Université Paris Diderot, CNRS/IN2P3, Paris, France)*
[66]*Institut für Physik, Universität Rostock, Rostock, Germany (associated with Physikalisches Institut, Ruprecht-Karls-Universität Heidelberg, Heidelberg, Germany)*
[67]*National Research Centre Kurchatov Institute, Moscow, Russia [associated with Institute of Theoretical and Experimental Physics (ITEP), Moscow, Russia]*
[68]*Instituto de Fisica Corpuscular (IFIC), Universitat de Valencia-CSIC, Valencia, Spain (associated with ICCUB, Universitat de Barcelona, Barcelona, Spain)*
[69]*Van Swinderen Institute, University of Groningen, Groningen, Netherlands (associated with Nikhef National Institute for Subatomic Physics, Amsterdam, Netherlands)*

[†]Deceased.
[a]Universidade Federal do Triângulo Mineiro (UFTM), Uberaba-MG, Brazil.
[b]Laboratoire Leprince-Ringuet, Palaiseau, France.
[c]P.N. Lebedev Physical Institute, Russian Academy of Science (LPI RAS), Moscow, Russia.
[d]Università di Bari, Bari, Italy.
[e]Università di Bologna, Bologna, Italy.
[f]Università di Cagliari, Cagliari, Italy.
[g]Università di Ferrara, Ferrara, Italy.
[h]Università di Genova, Genova, Italy.
[i]Università di Milano Bicocca, Milano, Italy.
[j]Università di Roma Tor Vergata, Roma, Italy.
[k]Università di Roma La Sapienza, Roma, Italy.
[l]AGH University of Science and Technology, Faculty of Computer Science, Electronics and Telecommunications, Kraków, Poland.

[m]LIFAELS, La Salle, Universitat Ramon Llull, Barcelona, Spain.
[n]Hanoi University of Science, Hanoi, Vietnam.
[o]Università di Padova, Padova, Italy.
[p]Università di Pisa, Pisa, Italy.
[q]Università degli Studi di Milano, Milano, Italy.
[r]Università di Urbino, Urbino, Italy.
[s]Università della Basilicata, Potenza, Italy.
[t]Scuola Normale Superiore, Pisa, Italy.
[u]Università di Modena e Reggio Emilia, Modena, Italy.
[v]Iligan Institute of Technology (IIT), Iligan, Philippines.
[w]Novosibirsk State University, Novosibirsk, Russia.